

STAR FORMATION IN SELF-GRAVITATING TURBULENT FLUIDS

NORMAN MURRAY^{1,2} & PHILIP CHANG³,
Draft version July 25, 2014

ABSTRACT

We present a model of star formation in self-gravitating turbulent gas. We treat the turbulent velocity v_T as a dynamical variable, and assume that it is adiabatically heated by the collapse. The theory predicts the run of density, infall velocity, and turbulent velocity, and the rate of star formation in compact massive gas clouds. The turbulent pressure is dynamically important at all radii, a result of the adiabatic heating. The system evolves toward a coherent spatial structure with a fixed run of density, $\rho(r, t) \rightarrow \rho(r)$; mass flows through this structure onto the central star or star cluster. We define the sphere of influence of the accreted matter by $m_* = M_g(r_*)$, where m_* is the stellar plus disk mass in the nascent star cluster and $M_g(r)$ is the gas mass inside radius r . The density is given by a broken power law with a slope -1.5 inside r_* and ~ -1.6 to -1.8 outside r_* . Both v_T and the infall velocity $|u_r|$ decrease with decreasing r for $r > r_*$; $v_T(r) \sim r^p$, the size-linewidth relation, with $p \approx 0.2 - 0.3$, explaining the observation that Larson's Law is altered in massive star forming regions. The infall velocity is generally smaller than the turbulent velocity at $r > r_*$. For $r < r_*$, the infall and turbulent velocities are again similar, and both increase with decreasing r as $r^{-1/2}$, with a magnitude about half of the free-fall velocity. The accreted (stellar) mass grows super-linearly with time, $\dot{M}_* = \phi M_{\text{cl}}(t/\tau_{\text{ff}})^2$, with ϕ a dimensionless number somewhat less than unity, M_{cl} the clump mass and τ_{ff} the free-fall time of the clump. We suggest that small values of p can be used as a tracer of convergent collapsing flows.

1. INTRODUCTION

The importance of massive stars in a human context became apparent when Burbidge et al. (1957) showed that such stars were responsible for the production and distribution of most of the heavy elements that composed the Earth, and which form the building blocks of life.

More recently it has emerged that massive stars are important on a less parochial scale. Star formation on galactic scales is observed to be slow, in the sense that the time to deplete the supply of gas from which stars are made is some fifty times the dynamical time. Quantitatively,

$$\dot{M}_* = \eta \frac{M_g}{\tau_{\text{DYN}}}, \quad (1)$$

where $\eta \approx 0.017$ is a dimensionless constant, and $\tau_{\text{DYN}} = R/v_c$ is the dynamical time of a galactic disk of radius R with circular velocity v_c (Kennicutt 1998; Leroy et al. 2008). Massive stars provide the feedback that limits the rate of star formation in galaxies. The feedback comes in the form of radiation pressure, gas pressures in ionized regions, blast waves from supernovae, and cosmic rays. The

feedback also drives gas out of galaxies, setting the stellar mass-halo mass relationship for halo masses $M_h \lesssim 10^{13} M_\odot$, e.g., Hopkins et al. (2013); Trujillo-Gomez et al. (2013); Agertz & Kravtsov (2014); Ceverino et al. (2014). Understanding how massive stars form is clearly important to our comprehension of the evolution of the universe, and many of its components.

Stars more massive than sixty solar masses ($M_* > 60 M_\odot$) live only 4 Myr. Since we see stars with masses in excess of $60 M_\odot$ outside their natal dense gas clumps, the early accretion rate onto such a star must exceed $\approx 3 \times 10^{-5} M_\odot \text{ yr}^{-1}$, where we have assumed that the most massive stars are visible for $\gtrsim 1$ Myr, hence they can accrete for no more than 3 Myr. In the Milky Way, these massive stars are usually found in compact 1 – 10 pc radius clusters containing up to $10^5 M_\odot$ of stars. The accretion rates for clusters must exceed a few hundredths of a solar mass per year, $\dot{M}_* \gtrsim 3 \times 10^{-2} M_\odot \text{ yr}^{-1}$. For example, Cygnus OB2 contains $M_* \gtrsim 4 - 10 \times 10^4 M_\odot$ inside a half light radius $r_h = 6.4$ pc (Knödlseeder 2000), yielding $\dot{M}_* \approx 0.02 M_\odot \text{ yr}^{-1}$. The free-fall time of the natal cluster is

$$\begin{aligned} \tau_{\text{ff}} &\equiv \sqrt{\frac{3\pi}{32G\rho}} \\ &= 1 \left(\frac{3 \times 10^4 M_\odot}{M_*} \right)^{-1/2} \left(\frac{R_{1/2}}{6.4 \text{ pc}} \right)^{3/2} \left(\frac{\epsilon}{0.5} \right) \text{ Myr}, \end{aligned}$$

where all quantities are estimated at the half light

¹ Canadian Institute for Theoretical Astrophysics, 60 St. George Street, University of Toronto, Toronto ON M5S 3H8, Canada; murray@cita.utoronto.ca

² Canada Research Chair in Astrophysics

³ Department of Physics, University of Wisconsin-Milwaukee, 1900 E. Kenwood Blvd., Milwaukee, WI 53211, USA; chang65@uwm.edu

radius, and $\epsilon \equiv \dot{M}_*/M_g$ is the fraction of natal gas in a dense cluster-forming region that is converted into stars. The star formation rate per free fall time, the small-scale analog of η in eqn (1), is

$$\begin{aligned} \epsilon_{\text{ff}} &\equiv \frac{\dot{M}_*}{\tau_{\text{ff}} M_g} = \frac{\tau_{\text{ff}}}{3 \text{ Myr}} \epsilon \\ &\approx 0.16 \left(\frac{R_{1/2}}{6.4 \text{ pc}} \right)^{3/2} \left(\frac{M_{*,1/2}}{3.5 \times 10^4 M_\odot} \right)^{1/2} \left(\frac{\epsilon}{0.5} \right)^{1/2} \end{aligned} \quad (2)$$

This estimate of ϵ_{ff} is consistent with many estimates in the literature, for example, Wu et al. (2005), Lada et al. (2010), Heiderman et al. (2010), and Murray (2011), although there is some disagreement, e.g., (Krumholz et al. 2012a).

The fact that $\epsilon_{\text{ff}} \gg \eta$ is one of the reasons that astronomers believe that stellar feedback is necessary to explain the slow global rate of star formation; if $\epsilon_{\text{ff}} = \eta$, no feedback would be required. A second motivation for feedback is that simulations on the scale of galaxies, and on the scale of star forming clumps ($r \sim 1 - 10 \text{ pc}$) both find very rapid star formation if no feedback is included.

In this paper we are interested in the physics behind rapid star formation rather than the physics of feedback. The problem arises from the high accretion rates, discussed above, required to make massive stars. The early model of Shu (1977) gave an estimate of the star formation rate. His model assumed that stars formed from hydrostatic cores supported by thermal gas pressure. The accretion rate in his model was independent of time, given by $\dot{M}_* = m_0 c_s^3 / G$, where $c_s \approx 0.2 \text{ km s}^{-1}$ is the sound speed in molecular gas, and $m_0 = 0.975$. Thus the maximum accretion rate was $\dot{M}_* \approx 2 \times 10^{-6} M_\odot \text{ yr}^{-1}$, too small by a factor of ten to explain the origin of massive stars.

The difficulty with the accretion rate was overcome by Myers & Fuller (1992), who noted that cores in massive star forming regions had linewidths that exceeded the thermal line width by factors of several or more. They pointed out that the accretion rate in Shu's model was limited by the signal speed of the expanding collapse wave, then took advantage of the larger signal speed available if they assumed that the pressure in the fluid was given by

$$P(r, t) = \rho(r, t) [c_s^2 + v_T^2(r)], \quad (3)$$

where $\rho(r, t)$ is the local density, c_s is the sound speed, and $v_T(r)$ is the turbulent velocity a distance r from the center of the collapse.

The model was further developed by McLaughlin & Pudritz (1997) and McKee & Tan (2003). These models kept some of the features of Shu's model, including the assumption of a hydrostatic initial core, and the static nature of the turbulent velocity in the equation of state (3). In particular, they assumed that v_T was not affected by the collapse, and that it was independent of time. They did not address the question of how a hydrostatic core was assembled.

Observations in large GMCs, and low mass cores, find

$$v_T(r) = v_T(R) \left(\frac{r}{R} \right)^p \quad (4)$$

with $p \approx 0.5$ (Larson 1981; Myers & Goodman 1988); as we will discuss further below, in massive star forming regions v_T behaves differently, with $p \approx 0.2$ and much larger turbulent velocities at a given separation r than in low mass star forming regions. The turbulent core models either explicitly assume a turbulent velocity of the form (4), or assumed implicitly that it follows a power law in radius so that $P(r) \sim \rho^\gamma(r)$.

In a companion paper (Lee et al. 2014) (Paper I) we present three dimensional hydro and MHD simulations which recover the result $p \approx 0.5$ in the bulk of the gas. However, we also show that in small regions around density peaks, which we identify as cores, $p \approx 0.2$.

In this paper we assume that massive stars form in regions of turbulent flows in which the gas is converging, so that there is never any time at which the region is in hydrostatic equilibrium. The infall therefore extends over a much larger region than that envisioned in the hydrostatic turbulent core models.

A more profound difference arises from the fact that we model the turbulent velocity $v_T(r, t)$ as a dynamical variable, changing in response to the evolution of the system. This requires that we introduce a third dynamical equation, the energy equation. However, we are unable to solve the equations that result. This is not surprising, because numerical solutions of the full set, carried out in three dimensions, show that the motion becomes turbulent.

Suitably chastened, we then make two simplifications. First, we assume spherical symmetry, reducing the problem from three spatial dimensions to one. Second, we introduce a closure for the energy equation, that proposed by Robertson & Goldreich (2012).

We import the notion of the sphere of influence of the star from galactic dynamics, and define the radius $r_*(t)$ at which the mass of gas just equals the (time dependent) mass of the star. With our two assumptions, and the concept of the sphere of influence, we are able to find self-similar solutions that describe the collapse of a self-gravitating turbulent gas. We calculate the run of density $\rho(r, t)$, of infall velocity $u_r(r, t)$, and of the turbulent velocity $v_T(r, t)$. We find the striking result that for $r < r_*(t)$, the density approaches a fixed function of radius, independent of time, i.e., $\rho(r, t) \rightarrow \rho_*(r) \sim r^{-3/2}$. For $r > r_*$, $\rho(r, t) \sim r^{-k_\rho}$, with $k_\rho \approx 1.6 - 1.8$.

We show that the acceleration due to the pressure gradient always tracks the acceleration of gravity. For $r < r_*(t)$, the result is that both the infall velocity and the turbulent velocity increase with decreasing radius, as $r^{1/2}$. But for $r > r_*(t)$, the pressure

force exceeds that due to gravity. As a result, both $v_T(r, t)$ and $u_r(r, t)$ increase slowly with increasing radius, $v_T(r, t) \sim r^p$, with $p \approx 0.2$. This appears to explain the deviations from Larson’s size-linewidth relation seen in massive star forming regions.

It follows from the fact that the density is independent of time for $r < r_*$, and from $u_r(r, t) \sim \sqrt{GM_*/r}$, that the mass accretion rate increases linearly with time, so that

$$M_* = \phi M_{cl} \left(\frac{t - t_*}{\tau_{ff}} \right)^2, \quad (5)$$

where M_{cl} is the mass of the star forming clump, and τ_{ff} is the free fall time of the clump.

This paper is organized as follows. In §2 we present a spherically symmetric one dimensional model for the collapse of a turbulently supported gas cloud consisting of the continuity and momentum equations, and a simple closure for the energy equation. We describe approximate analytic solutions to these equations, and comment on the effects of thermal and magnetic support. In §3 we solve the equations numerically. In §4 we briefly compare observations of infall in the massive star forming regions, with special attention given to G10.6-0.4. We also discuss previous analytic and numerical work. We wrap up with our conclusions in the final section.

2. SPHERICAL GRAVITATIONAL COLLAPSE MODELS

The governing equations are the continuity equation

$$\frac{\partial \rho}{\partial t} + \nabla \cdot (\rho \mathbf{u}) = 0, \quad (6)$$

the momentum equation

$$\frac{\partial \rho \mathbf{u}}{\partial t} + \nabla \cdot \rho \mathbf{u} \mathbf{u} = -\nabla P + \rho \mathbf{g}, \quad (7)$$

and the energy equation

$$\begin{aligned} \frac{\partial}{\partial t} \left[\rho \left(\frac{1}{2} u^2 + \mathcal{E} \right) \right] + \nabla \cdot \left[\rho \left(\frac{1}{2} u^2 + \mathcal{E} \right) \cdot \mathbf{u} + \mathbf{u} P \right] \\ = \rho \mathbf{g} \cdot \mathbf{u}. \end{aligned} \quad (8)$$

In these equations ρ is the density, \mathbf{u} is the fluid velocity, P is the gas pressure, \mathbf{g} is the acceleration due to gravity, and \mathcal{E} is the internal energy of the gas.

In the companion paper (Paper I), we solve these equations via a three dimensional simulation. In this paper, we simplify our model to gain some physical insight into the collapse process. To do so we will simplify the energy equation. We start by noting that simulations of both supersonic and subsonic turbulence have generally found that the properties of the turbulent flow are universal, in the sense that certain relations are found under a wide variety of conditions. In particular, simulations find velocity power spectra that have approximate power law

forms, e.g., $P_v(k) \sim k^{-5/3}$ for subsonic turbulence or $P_v(k) \sim k^{-2}$ for supersonic turbulence. Correspondingly, $v_T(r) \sim r^{1/3}$ or $v_T(r) \sim r^{1/2}$.

It is tempting to conclude that the energy equation can be replaced by a simple closure relation specifying the turbulent velocity, namely $v_T(r, t) = v_T(r)$, where $v_T(r)$ is given by Larson’s law. This is what has been done in most previous analytic work on turbulent collapse.

This temptation should be resisted. It is well known that turbulence decays on a turnover time $r/v_T(r)$, and it is believed that in star forming galaxies the energy lost in this decay is replaced by stellar feedback, e.g., from supernovae. One could argue that this leads to a steady state, i.e., that $v_T(r, t) = v_T(r)$. However, Robertson & Goldreich (2012) showed that compression of turbulent gas also drives turbulence. Turbulent gas in a converging flow will be compressed, which tends to increase v_T , while v_T will also decay due to dissipation. Therefore, we use a closure scheme suggested by Robertson & Goldreich (2012) that captures both the decay and the compressive driving.

In the absence of collapse, undriven turbulence decaying on an eddy turnover time is described by

$$\frac{1}{2} \frac{dv_T^2(r)}{dt} = -\eta \frac{v_T^3}{r}, \quad (9)$$

with η a dimensionless constant of order unity.

Collapse alters the turbulence. Ignoring for the moment the cascade of energy from large scales to small that is responsible for (9), a reduction in the radius from R to r results in a scaling of the velocity $v_T(r) = v_T(R) \times (R/r)$, i.e.,

$$\left(\frac{dv_T}{dt} \right)_{AH} = -v_T \frac{u_r}{r}, \quad (10)$$

where $u_r = dr/dt$ is negative for a collapse. Thus the scaling relation suggests that a collapse will tend to increase the turbulent velocity. Robertson & Goldreich refer to this as “adiabatic heating”, and show that such heating occurs in cosmological simulations in which the scale factor decreases with time, mimicking a gravitational collapse.

Combining this driving term with the turbulent damping,

$$\frac{dv_T}{dt} = - \left(1 + \eta \frac{v_T}{u_r} \right) \frac{v_T u_r}{r}. \quad (11)$$

We use this equation to replace the energy Equation (8).

2.1. Fundamental Equations

In Paper I we show that on parsec and smaller scales, the collapse is, very roughly, spherically symmetric. Motivated by this and our desire to simplify our model, we employ spherical coordinates. Both simulations and observations of star forming regions show the presence of star forming regions that have cylindrical geometry, as well as other regions with

spherical geometry, or a combination of both. We have made some initial forays into cylindrical geometry, but for simplicity we stick to spherical geometry in this paper.

The continuity and momentum equations become

$$\frac{\partial \rho}{\partial t} + \frac{1}{r^2} \frac{\partial}{\partial r} (r^2 u \rho) = 0, \quad (12)$$

and

$$\frac{\partial u_r}{\partial t} + u_r \frac{\partial u_r}{\partial r} + \frac{1}{\rho} \frac{\partial \rho (v_T^2(r, t) + c_s^2)}{\partial r} + \frac{GM(r, t)}{r^2} = 0, \quad (13)$$

while the energy equation is

$$\frac{\partial v_T}{\partial t} + u_r \frac{\partial v_T}{\partial r} + \left(1 + \eta \frac{v_T}{u_r}\right) \frac{v_T u_r}{r} = 0. \quad (14)$$

In these equations $u_r(r, t)$ is the mean radial velocity of the fluid, excluding the turbulent velocity, which is denoted by $v_T(r, t)$. In the rest of this section only, we will neglect the sound speed c_s to simplify the presentation. In any case, we find that its inclusion has little effect on the results.

The mass $M(r, t) = M(0, t) + M_g(r, t)$ where

$$M_g(r, t) = 4\pi \int_{0+}^r r^2 \rho(r, t) dr \quad (15)$$

is the gas mass.

We will employ $M_*(t)$ rather than $M(0, t)$, with the understanding that M_* may refer to the mass of a single star or to a star cluster. For later use we define the radius or sphere of influence of the nascent star or star cluster by

$$M_*(t) = 4\pi \int_{0+}^{r_*(t)} r^2 \rho(r, t) dr. \quad (16)$$

Thus $r_*(t)$ is the radius at which the enclosed gas mass equals the mass in stars; this makes sense if the distribution of young stars is more centrally concentrated than the gas, which is true on large enough scales. For a pure power law density distribution $\rho(r) \sim r^{-k_\rho}$,

$$r_*(t) = R \left[\frac{M_*(t)}{M_{cl}} \right]^{1/(3-k_\rho)}, \quad (17)$$

where R is a fiducial radius, and M_{cl} is the mass of gas inside that radius. We have in mind the thickness of the ribbon-like features found in hydrodynamic simulations, e.g., those in paper I, for R .

2.2. Solution

We will concentrate on a solution from the time when a star first forms. We define scaled variables

$$x \equiv \frac{r}{r_0} \quad (18)$$

and

$$y \equiv \frac{t}{\tau_{\text{DYN}}}, \quad (19)$$

where r_0 is a fiducial radius, and $\tau_{\text{DYN}} = R/u_r(R)$.

We define

$$p \equiv \frac{r}{v_T} \frac{\partial v_T}{\partial r}, \quad p' \equiv \frac{r}{u_r} \frac{\partial u_r}{\partial r}, \quad \text{and} \quad k_\rho \equiv -\frac{r}{\rho} \frac{\partial \rho}{\partial r}, \quad (20)$$

anticipating that each will vary only slowly with radius. In other words, we look for solutions in which the density, infall velocity, and turbulent velocity are all approximately power laws in both r and t ,

$$\rho(r, t) = \rho_0 x^{-k_\rho} y^\alpha, \quad (21)$$

$$u_r(r, t) = u_0 x^{p'} y^\beta, \quad (22)$$

and

$$v_T(r, t) = v_0 x^p y^\gamma. \quad (23)$$

where we have defined $\rho_0 \equiv \rho(r_0, \tau_{\text{DYN}})$, with similar expressions for u_0 and v_0 .

For an infall solution, we expect that the magnitude of the infall velocity increases with time; mass accumulates in the central object, which then exerts a gravitational force on the surrounding material that increases with time. Our energy closure then ensures that the turbulent velocity will increase (at a fixed radius) with increasing time, so that

$$\beta > 0, \quad \gamma > 0. \quad (24)$$

We define $\tilde{\rho}(t) \equiv \rho_0 y^\alpha$, so that $\rho(r, t) = \tilde{\rho}(t) x^{-k_\rho}$.

2.3. Solution at Small Radius, $r < r_*(t)$

The continuity equation becomes

$$\frac{\partial \tilde{\rho}}{\partial t} x^{-k_\rho} + \frac{u_0 \rho_0}{r_0} x^{p' - k_\rho - 1} y^{\alpha + \beta} [2 + p' - k_\rho] = 0. \quad (25)$$

As $r \rightarrow 0$, the second term grows more rapidly than the first term, since $p' < 1$; in fact we will show that $p' = -1/2$. Thus at small radii ($r \ll r_*$) satisfying this equation demands that both terms go to zero independently. For the larger, second term, this implies

$$k_\rho = 2 + p'. \quad (26)$$

Similarly, for the first term, we find

$$\frac{\partial \rho(r, t)}{\partial t} = 0. \quad (27)$$

This is a very striking result: self-similar gravitational collapse (in which the density and infall velocity follow power laws in radius) evolves to an attractor, in which the density does not vary with time. Note that the argument has made no reference to the type of pressure support, i.e., thermal, turbulent, or magnetic.

2.3.1. Using the energy closure to relate u_r to v_T

Using the power law ansatz, Equation (14) becomes

$$\gamma \frac{v_0}{\tau_{\text{DYN}}} y^{\gamma-1} x^p + \frac{u_0 v_0}{r_0} y^{\beta+\gamma} x^{p+p'-1} \times \left[p + 1 + \left(\frac{v_T(r, t)}{u_r(r, t)} \right) \eta \right] = 0. \quad (28)$$

We can then show

$$v_T(r, t) = -u_r(r, t) \frac{1+p}{\eta} - \frac{\gamma r}{\eta t}. \quad (29)$$

At small r and large t , the result (29) implies that $v_T \sim u_r$, so that (29) is the analog of the result in Robertson & Goldreich (2012) that $v_T \sim a^{\tilde{\beta}-1}$, where a is the scale factor in their cosmological simulations and $\tilde{\beta}$ is given by their Equation (9). We note that this result implies

$$p = p', \quad \beta = \gamma, \quad \text{for } r < r_*. \quad (30)$$

2.3.2. The Momentum Equation at Small Radii

We start by noting that

$$M(r, t) = M_*(t) + \frac{4\pi}{3-k_\rho} r_0^3 \rho_0 x^{3-k_\rho}, \quad (31)$$

where the second term on the right hand side does not depend on time, a result that follows from equation (27).

The momentum equation is

$$\left(\frac{u_0}{\tau_{\text{DYN}}} y^{\beta-1} x^{p'} + \frac{4\pi G \rho_0 r_0}{3-k_\rho} x^{1-k_\rho} \right) + \left[\frac{u_0^2}{r_0} p' y^{2\beta} x^{2p'-1} + \frac{v_0^2}{r_0} (2p-k_\rho) y^{2\gamma} x^{2p-1} + \frac{GM_*(t)}{r_0^2} x^{-2} \right] = 0. \quad (32)$$

We have written equation (32) so as to group together terms that scale with r in the same manner. From equations (25) and (30), $1-k_\rho = -(1+p)$; since we expect gravity to cause the infall to increase the magnitude of u_r as r decreases, $p' = p < 0$. It follows that $r^{1-k_\rho} = r^{-1-p} < r^{2p-1}$, i.e., the pressure gradient term is larger in magnitude than the gas self-gravity term, and also larger than $|\partial u_r / \partial t|$. The pressure gradient term and the advective term must together balance the stellar gravitational term, so we group those three terms together in the square brackets. On setting the sum of the three terms to zero, we have

$$u_r = -\Gamma \sqrt{\frac{GM_*(t)}{r}}, \quad (33)$$

where we have used Equation (29), and defined

$$\Gamma \equiv \left[(k_\rho - 2p) \left(\frac{1+p}{\eta} \right)^2 - p' \right]^{-1/2}. \quad (34)$$

Combining Equation (33) with Equation (26) shows that

$$p' = p = -\frac{1}{2}, \quad k_\rho = 3/2, \quad (r < r_*). \quad (35)$$

Equation (33) also shows that $M_*(t) \sim t^{2\beta}$.

The remaining two terms, the time rate of change of u_r and the gas self-gravity, inside the parentheses in equation (32) must separately cancel, or

$$\frac{\partial u_r}{\partial t} = -\frac{4\pi G \rho(r_0) r_0}{3-k_\rho} x^{1-k_\rho}. \quad (36)$$

This shows that the infall velocity increases linearly with time ($\beta = 1$) after the central object forms. Integrating,

$$u_r(r, t) = u_r(r, 0) - \frac{4\pi G \rho(r_0) r_0}{3-k_\rho} x^{-1/2} t. \quad (37)$$

The two expression (33) and (37) must agree at late times, so that:

$$M_*(t) = \Gamma^{-2} \left(\frac{4\pi \rho(r_0)}{3-k_\rho} \right)^2 G r_0^3 t^2. \quad (38)$$

We show in the next section that $k_\rho \approx 1.6 - 1.7$ for $r > r_*$. This allows us to connect the density at any $r < r_*$ to the density $\rho(R)$ at $r = R$,

$$\begin{aligned} \rho(r) &= \rho(R) \left(\frac{r}{r_*} \right)^{-3/2} \left(\frac{r_*}{R} \right)^{-k_\rho} \\ &= \rho(R) \left(\frac{r}{R} \right)^{-3/2} \cdot \left(\frac{r_*}{R} \right)^{3/2-k_\rho} \end{aligned} \quad (39)$$

The fact that $3/2 - k_\rho \ll 1$ suggests that we define

$$\psi(k_\rho, r_*(t)) \equiv \left(\frac{r_*}{R} \right)^{3/2-k_\rho}. \quad (40)$$

Because $k_\rho - 3/2 \approx 0.1$, the dependence of ψ on r_* is very weak; if $r_* = 10^{-5} R$, $\psi = 3$.

Using this, the stellar mass at time t can be written in terms of the clump mass as

$$M_*(t) = \psi \cdot \left(\frac{\pi}{2\Gamma} \right)^2 M_{cl} \left(\frac{t-t_*}{\tau_{\text{ff}}} \right)^2, \quad (41)$$

where we now explicitly display t_* , the time at which the central density diverges, or that at which the central star forms.

It follows that

$$r_*(t) = \psi^{2/3} \cdot \left[\frac{\pi}{2\Gamma} \right]^{4/3} \left(\frac{t-t_*}{\tau_{\text{ff}}} \right)^{4/3} R, \quad (42)$$

where to a first approximation it is acceptable to treat ψ as a constant, independent of both r_* and time.

It is instructive to compare the acceleration terms in the momentum equation, normalizing to $g \approx GM_*(t)/r^2$. The acceleration due to the pressure gradient is

$$\frac{1}{g} \left(\frac{1}{\rho} \frac{\partial P}{\partial r} \right) \approx (2p-k_\rho) \left(\frac{v_T}{u_r} \right)^2 \Gamma^2 \approx -\frac{5}{5+4\eta^2}, \quad (43)$$

while the net acceleration of the gas is approximately

$$\frac{1}{g} \frac{du_r}{dt} \approx p' \Gamma^2 \approx -\frac{4\eta^2}{5+4\eta^2}. \quad (44)$$

For $\eta = 2/3$, the ratio between the acceleration due to the pressure gradient and gravity is $(\partial P/\partial r)/\rho g \approx 0.74$ (equation [43]), i.e., they nearly balance each other. Hence, the net acceleration of the gas is only roughly one quarter that of gravity. In other words, for $r < r_*$, gravity dominates the dynamics, but it is nearly balanced by turbulent pressure, and the infall velocity is substantially smaller than the free fall velocity.

In the next section we show that for $r > r_*$, both p' and p are greater than zero; the turbulent pressure decelerates the infall, and the turbulent velocity tracks the infall velocity, as prescribed by Equation (11). As the flow crosses r_* , the acceleration due to gravity, which we will show scales as $\sim r^{-0.6}$ for $r > r_*$, transitions to scaling as r^{-2} for $r < r_*$. The infall velocity responds to this increased gravity rapidly, i.e. in a moderately small fraction of the local dynamical time; the turbulent velocity follows, but with a substantial lag (of order the local dynamical time), eventually reaching $p = p'$, as enforced by our energy closure, Equation(11). The acceleration due to the pressure gradient tracks that due to gravity at all radii. However for $r > r_*$ the pressure term dominates the gravity term, while for $r < r_*$, the gravity term is roughly twice the pressure term, as we have just seen.

2.3.3. Summary at $r \ll R$

Gathering the results, we have shown that the turbulent velocity tracks the infall velocity, that $k_\rho = 2 + p'$ (from the continuity equation), and $p' = -1/2$ for $r < r_*(t)$; it follows that $k_\rho = -3/2$ for $r < r_*(t)$.

The mass accretion rate for $r < r_*(t)$ is roughly independent of radius,

$$\begin{aligned} \frac{dM_g(r,t)}{dt} &= 4\pi r^2 \rho(r,t) u_r(r,t) \\ &\approx 4\pi r_0^2 \rho_f(r_0) u_r(r_0, t), \end{aligned} \quad (45)$$

where we used the fact that $2 - k_\rho + p' = 0$ for $r < r_*$.

Although the density $\rho(r,t) = \rho(r)$, i.e., it is independent of time, the accretion rate does vary with time since the infall velocity $u_r(t,r)$ does. In other words, the accretion rate does not vary with radius (for $r < r_*$) at a fixed time, but it does increase linearly with time at a fixed radius.

2.4. Solution for $r_* < r \lesssim R$

It is useful to define times scales for the density, radial velocity, and turbulent velocity to change by a factor of order unity:

$$\tau_\rho \equiv \left(\frac{1}{\rho} \frac{\partial \rho}{\partial t} \right)^{-1}, \quad (46)$$

$$\tau_{u_r} \equiv \left(\frac{1}{u_r} \frac{\partial u_r}{\partial t} \right)^{-1}, \quad (47)$$

and

$$\tau_{v_T} \equiv \left(\frac{1}{v_T} \frac{\partial v_T}{\partial t} \right)^{-1}. \quad (48)$$

Well away from $r = r_*$ and $r = R$, we expect that these should be of order the local dynamical time

$$\tau_{\text{dyn}} \equiv \frac{r}{v_r}. \quad (49)$$

The momentum equation can be written as

$$\frac{\tau_{\text{dyn}}}{\tau_{u_r}} + p' + \left(\frac{v_T}{u_r} \right)^2 (2p - k_\rho) + \left(\frac{v_T}{u_r} \right)^2 \frac{GM/r}{v_T^2} = 0. \quad (50)$$

Since the turbulent velocity tracks the infall velocity, v_T/u_r varies slowly with r ; for $r_* \ll r \ll R$, we expect $\tau_{\text{dyn}}/\tau_{u_r}$ to vary slowly with r as well. Then

$$v_T(r,t) = \Gamma' \sqrt{\frac{GM(r,t)}{r}}, \quad (51)$$

where

$$\Gamma' \equiv \left| \frac{v_T}{u_r} \right| \Gamma = \left[k_\rho - 2p - \left(p' + \frac{\tau_{\text{dyn}}}{\tau_{u_r}} \right) \left(\frac{u_r}{v_T} \right)^2 \right]^{-1/2} \quad (52)$$

is a slowly varying function of r for $r > r_*$. Note that $\Gamma'^2 \approx \alpha_{\text{vir}}$, the virial parameter.

Because Γ' is a slowly varying function of r , it follows from Equation (51) that

$$2p = 2 - k_\rho, \quad r > r_*. \quad (53)$$

The continuity equation can be written as

$$\frac{\tau_{\text{dyn}}}{\tau_\rho} + 2 + p' - k_\rho = 0. \quad (54)$$

Combining this with Equation (53), we find

$$p' = \left| \frac{\tau_{\text{dyn}}}{\tau_\rho} \right| - 2p, \quad r > r_*. \quad (55)$$

In the appendix we argue that if the outer boundary condition on the density is $\rho(R,t) = \bar{\rho}$, we can approximate

$$\left| \frac{\tau_{\text{dyn}}}{\tau_\rho} \right| \approx \left| \frac{\ln r/r_*}{\ln R/r_*} - 1 \right|. \quad (56)$$

In the Appendix we show that

$$p(r) = \frac{1}{2} k_\rho - \frac{1}{2} \left(\frac{u_r}{v_T} \right)^2 \left[\frac{\tau_{\text{dyn}}}{\tau_{u_r}} + p' + \Gamma^{-2}(0) \right], \quad (57)$$

and estimate $p \approx 0.1 - 0.2$.

From Equation (53), we find

$$k_\rho \approx 1.6 - 1.8, \quad (58)$$

again depending on the initial conditions and on η .

Unlike the case at $r < r_*$, here the dynamics are controlled by the pressure gradient, and not by gravity. The ratio

$$\frac{1}{g} \left(\frac{1}{\rho} \frac{\partial P}{\partial r} \right) = -(k_\rho - 2p)\Gamma'^2 \approx -3 \text{ to } -4 \quad (59)$$

for $v_T \approx 1.6\sqrt{GM(R)/R}$, the fiducial value used in the numerical simulations below, and $p \approx 0 - 0.2$, motivated by the results of the Appendix.

The force due to the steep pressure gradient (or more precisely the density gradient, since $k_\rho \gg |2p|$) is larger than the force of gravity. This outward-directed force causes the infall velocity to decrease inward, for $r_* < r \ll R$. This is quantified by combining Equation (55) with Equation (56). At $r_* \lesssim r \ll R$, we expect $p' \approx 1 - 2p > 0$, so that $|u_r|$ decreases with decreasing radius.

This result, that $|u_r|$ decreases inward for $r > r_*$, is in contrast to self-similar solutions with an assumed fixed turbulent velocity. In such theories, the infall velocity is either zero outside the radius of the expanding collapse wave (Shu 1977; McKee & Tan 2003) or has a magnitude that *increases* inward even at large radii (Fatuzzo et al. 2004).

In the next section, we use direct numerical integration of the 1D equations to show that $0.1 \lesssim p \lesssim 0.25$, depending on the outer boundary conditions and on η , similar to the result of 3D simulations in Paper I.

This value of the turbulent exponent is much smaller than the exponent in non-self-gravitating supersonic turbulence, $p = 1/2$, and smaller than the Kolmogorov value $p = 1/3$ for subsonic turbulence. Recall that the Kolmogorov value follows from conservation of energy in the cascade from large scales to small scales. In the case of supersonic collapse, the exponent is smaller than the value one would derive under the assumption that the kinetic energy in the cascade is conserved. Thus, the kinetic energy on small scales is larger than that produced by an energy conserving cascade.

The reason is simple: a fraction of the ordered inflow kinetic energy, and a fraction of the potential energy released in the collapse, is being converted into turbulent kinetic energy. In our simple theory, this fraction is set by the closure relation, Equation (11), which captures the behavior seen in the numerical simulations of Robertson & Goldreich (2012). This extra energy input boosts the turbulent velocity relative to that in an energy conserving cascade.

Inside the sphere of influence r_* the conversion of gravitational potential energy into turbulent energy is even more dramatic, as we saw above ($p = -1/2$), so that the turbulent velocity *increases* with decreasing r .

Simulations of non-self-gravitating turbulence consistently show $p \approx 0.5$, as do observations of GMCs (Larson 1981; Heyer & Brunt 2004) and low mass star formation regions (Myers 1983; Falgarone et al. 1992) in the Milky Way. We suggest that mea-

surements of the scaling of turbulent velocity can be used as a sign post for collapse, a point we return to below.

As in the case $r < r_*$, we have found that the dynamics converges to a run of density that varies only on the large scale dynamical time. In this case (for $r > r_*$) k_ρ is slightly larger than the value $k_\rho = 1.5$ found for $r < r_*$.

Unlike the small r case, however, we also find that the run of velocity (either $u_r(r)$ or $v_T(r)$) evolves rapidly to a solution that varies only on the dynamical time evaluated at the outer scale R , i.e., for $r_* < r < R$ the velocity increases only very slowly with time. This variation, on the global dynamical time, is simply a result of the change in the mass contained inside $r = R$. For $r_* \ll r \ll R$ the turbulent velocity is well described by a power law (with $p \approx 0.2$) while the infall velocity shows substantial deviations from a simple power law, as given by eqns. (55) and (56).

It follows that the mass accretion rate for $r > r_*$ varies fairly rapidly with radius,

$$\frac{dM_g(r, t)}{dt} = 4\pi r^2 \rho(R) u_r(R, t) \left(\frac{r}{R} \right)^{2-k_\rho+p'}, \quad (60)$$

where $2 - k_\rho + p' \approx 0.2 - 0.3$. We have allowed for the possibility that the infall velocity at R increases with time, as the growing mass of the clump will tend to accelerate the infall, but this increase is on the (large scale) dynamical time, and hence proceeds rather leisurely; essentially, the mass accretion rate is independent of time for $r > r_*$, but not for $r < r_*$!

In a more realistic model, including the effects of thermal gas pressure, magnetic pressure, and magnetic tension, as well as three dimensional effects, this mass accretion rate will be reduced. We discuss these effects briefly in the next subsection.

2.5. The Effects of Thermal and Magnetic Pressure, Rotation, and Magnetic Tension

There are several factors that will reduce the mass accretion rate in a more realistic model. First, we do not expect that gas will fall onto the star forming region from every direction, as we have assumed so far. In the three dimensional simulations in Paper I, we find that the infall covers a solid angle $\Omega_{in} < 4\pi$ steradians, which we account for by a factor $f_\Omega \equiv \Omega_{in}/(4\pi)$. In our MHD simulations, the fraction of the sky (as seen from the central object) over which accretion occurs is yet smaller, as the magnetic field line tension inhibits accretion across field lines, described by a factor $f_{\Omega_B} \leq 1$. Finally, the pressure associated with the magnetic field energy density provides an outward pressure gradient much like the turbulent pressure.

Rotational support will tend to slow the rate of accretion. However, observations suggest that the rotational velocity v_c in star forming cores is much smaller than the turbulent velocity, e.g., Beltrán et al. (2011); Palau et al. (2014), who find $v_c/v_T \lesssim$

0.3 at $r \approx 0.05$ pc. This appears to hold down to scales of order 1000AU or 5×10^{-3} pc, below which there is evidence for rotating disks, e.g., van der Tak et al. (2000).

We can include the effects of thermal pressure, and, in an approximate way, some of the effects of magnetic pressure and tension. All three tend to reduce the mass accretion rate, although for the massive star formation regions we consider here, with large virial velocities and high Mach numbers, the effects of thermal pressure are small.

The effects of magnetic pressure are potentially very significant. We expect that the strong turbulence generated in the converging flows we consider will tend to magnify the ambient magnetic field, possibly reaching equipartition, i.e., a magnetic pressure equal to ρv_T^2 , or a substantial fraction thereof. This effect can be incorporated in a very rough way by assuming a pressure of the form

$$P(r) = \rho(r) [c_s^2 + \phi_B v_T^2], \quad (61)$$

where $\phi_B = 1 + B^2/(8\pi\rho v_T^2)$. This expression does not entirely capture the effect of the magnetic pressure, since it implies that the magnetic field decays when the turbulent velocity does, contrary to what we expect. This might be important if the magnetic pressure becomes large enough to reduce the infall velocity of the flow; reducing u_r will reduce v_T , and hence in (61), the pressure associated with B . In fact, once the turbulence generates the magnetic field, the decay time of the magnetic field need not be related to the decay time of the turbulence.

We denote the fraction by which the magnetic pressure decreases the accretion rate by f_{B^2} ; we show below, using our simple model, that for a plasma $\beta \approx 1$, $f_{B^2} \approx 1/2$.

Accounting for all these effects, the expression for the stellar mass becomes

$$M_*(t) = f_\Omega f_{\Omega_B} f_{B^2} \psi \left(\frac{\pi}{2\Gamma} \right)^2 M_{\text{cl}} \left(\frac{t - t_*}{\tau_{\text{ff}}} \right)^2 \quad (62)$$

$$= \phi M_{\text{cl}} \left(\frac{t - t_*}{\tau_{\text{ff}}} \right)^2. \quad (63)$$

3. NUMERICAL RESULTS

We numerically integrate the full set of equations (12), (13), and (14), supplemented by (15) using a simple first order upwind code.

Our initial conditions are that the density is constant, $\rho(r, t = 0) = \bar{\rho}$, while the radial and turbulent velocities follow a power law,

$$u_r(r, t = 0) = -|u_r(R)| \left(\frac{r}{R} \right)^{p'} \quad (64)$$

and

$$v_T(r, t = 0) = v_T(R) \left(\frac{r}{R} \right)^p, \quad (65)$$

with fiducial values $\bar{\rho} = 3.0 \times 10^{-22}$ g s, $v_T(R) = 6.0$ km s $^{-1}$, $u_r(R) = -3.0$ km s $^{-1}$ and $p = p' = 1$.

The default value for the eddy decay time-scale is $\eta = 2/3$. We have explored variations around these fiducial values, and report on some of the results below. The boundary radius $R = 3 - 10$ pc for most of our runs. The initial mass is $M(R, 0) = 4\pi R^3 \bar{\rho}/3 \approx 1.8 \times 10^4 (R/10 \text{ pc})^3 M_\odot$, and the corresponding Keplerian velocity is

$$v_k(R, 0) = \sqrt{GM(R, 0)/R} \approx 2.8 \text{ km s}^{-1}. \quad (66)$$

Our outer boundary conditions specify the turbulent velocity and density, $v_T(R, t) = v_T(R)$ and $\rho(R, t) = \bar{\rho}$. The inflow velocity $u_r(R, t)$ is set to be a power law extrapolation of $u_r(R - dr, t)$, where dr is the grid scale. The inner boundary conditions are $u_r(r_{\text{in}}, t) = u_r(r_{\text{in}} + dr, t)$, $v_T(r_{\text{in}}, t) = v_T(r_{\text{in}} + dr, t)$, and $(r_{\text{in}})^2 \rho(r_{\text{in}}, t) = (r_{\text{in}} + dr)^2 \rho(r_{\text{in}} + dr)$, i.e., we insist that the mass flowing into the innermost shell $\dot{M}(r, t)$, which is deposited onto the central star, be the same as the mass flow rate into the surrounding shell.

We have integrated the equations both with and without including the effects of a finite sound speed. The results are virtually identical to those when the sound speed is neglected.

Figure 1 shows the run of density and infall velocity for fifteen snapshots between $t = 0 \tau_{\text{DYN}}$ and $t \approx 0.253 \tau_{\text{DYN}}$, where $\tau_{\text{DYN}} \equiv |R/u_r(R)|$. The first four snapshots show a core in the density distribution, $\rho(r) = \text{const.}$, with the constant increasing rapidly from 3×10^{-22} g cm $^{-3}$ in the initial snapshot to 10^{-16} g cm $^{-3}$ in the sixth snapshot. By the eighth snapshot, the density distribution has evolved into a (slightly broken) power law. The break in the power law occurs at $r = r_*(t)$; for $r < r_*(t)$, $\rho(r) \sim r^{1.5}$, while for $r > r_*(t)$, $\rho(r) \sim r^{k_\rho}$, with $k_\rho \approx 1.7$.

The infall velocity $-u_r(r, t)$ also evolves into a broken power law. For $r < r_*(t)$, the exponent $p' = -0.5$, while for $r > r_*(t)$, $p' \approx 0.2$, before flattening at $r \approx R$.

Figure 2 shows the ratio

$$\frac{(\nabla \rho v_T^2)/\rho}{GM(r, t)/r^2} \quad (67)$$

of the pressure gradient term to the gravity term in the momentum equation. We distinguish between times previous to the formation of the central object (shown by dotted lines) and times after the central object forms (shown by solid lines). These curves correspond to the same times as the curves in the previous figure.

At early times and small radii, the density is nearly constant, so $(1/\rho)dP/dr \sim dv_T^2/dr > 0$, and the pressure gradient provides an inward force, i.e., it acts in the same sense as gravity. Thus the pressure gradient force and the force due to gravity both act to move gas toward the origin. However, at large radii, the dotted curves drop down, eventually becoming negative at large radii, i.e., the pressure gradient term is directed outward, opposing the force

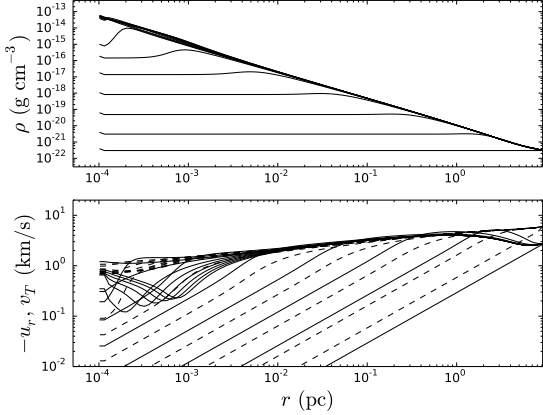


Figure 1. The run of density $\rho(r)$ (upper panel), infall velocity $-u_r(r)$ (lower panel, solid line), and turbulent velocity $v_T(r)$ (lower panel, dashed line) shown for 15 different times, ranging from the initial conditions to shortly after the formation of a star, which occurs at $t_*/\tau_{\text{dyn}} \approx 0.253$. The density increases from its initial value $\bar{\rho} = 3 \times 10^{-22} \text{ g cm}^{-3}$ to a maximum $\rho \approx 10^{-13} \text{ g cm}^{-3}$ at the inner edge of the integration region. Starting from the time just before the star forms, the density distribution is very nearly independent of time.

due to gravity. Near the outer boundary, this outward pressure gradient term is larger in magnitude than the acceleration of gravity.

After the first time step, the radius at which the pressure gradient changes sign is located at $r \approx 2 \text{ pc}$; well inside this radius, the density is uniform, $\rho(r) = \text{const}$. At each subsequent plotted time, the transition radius decreases by a factor of about three. Once again, at a fixed time, but well inside this transition radius, the density is uniform.

After the central object forms the situation is very different. To begin with, the pressure gradient is directed outward at all radii. However while the pressure gradient force is directed outward, it is smaller in magnitude than the force due to gravity at radii $r < r_*(t)$. Thus the infall velocity of a (Lagrangian) mass shell increases inward. The ratio of the two forces given by Equation (43) is constant, and is depicted in Figure 2 by the horizontal dashed line. The numerical result at late times (after the star forms) tracks this prediction for $r < r_*$. As a result, the infall velocity $u_r \sim r^{-1/2}$, but it is smaller than the free-fall velocity by a factor $\Gamma/\sqrt{2} \approx 1/2$. This is different than the prediction of the turbulent core model, in which the pressure term becomes negligible as $r \rightarrow 0$, so that the infall velocity approaches the free-fall value.

In contrast, for $r > r_*(t)$ the pressure gradient term is larger in magnitude than the gravity term, so that the infall velocity of a mass shell *decreases* inward. Note that the inertial term $u_r \partial u_r / \partial r$ is much smaller than either the pressure gradient term or the gravity term, or their difference, so that the infall velocity decreases in an Eulerian sense as well,

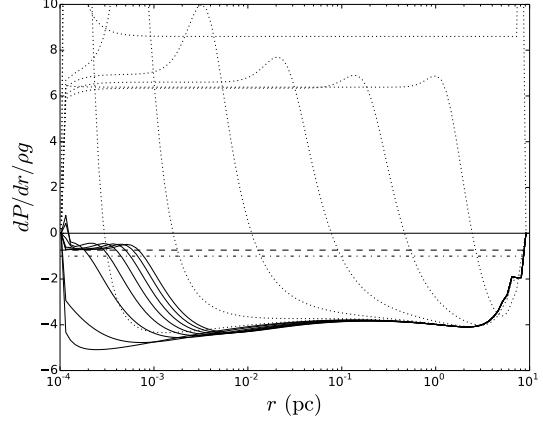


Figure 2. The ratio $(\partial \rho v_T^2 / \partial r) / (\rho G M(r, t) / r^2)$ plotted versus radius. The dotted (solid) lines correspond to times before (after) the central star forms. At large r the outward acceleration due to the pressure gradient exceeds the inward acceleration due to gravity (the dotted and solid lines are below the dot-dashed horizontal line at -1); this is why the infall velocity decreases inward for $r > r_*(t)$, as seen in figure 1. Inside $r_*(t)$, the acceleration due to the mass of the star exerts a gravitational force on the surrounding gas, but the star provides no outward pressure gradient; the small amount of gas between $r = r_{in}$ and r_* cannot provide a sufficiently strong pressure gradient, and so the magnitude of the infall velocity increases inward. However, even after the star forms, the acceleration provided by the pressure gradient is always a substantial fraction of the total gravitational acceleration—the solid lines are only slightly above the dot-dashed line for $r < r_*$. The horizontal dashed line is the prediction of Equation (43), at $-5/(5 + 4\eta^2)$, where in this case $\eta = 2/3$. For $r > r_*$, the ratio is roughly consistent with the prediction of Equation (59).

as seen in Figure 1.

Figure (3) shows Γ and Γ' . Note that Γ and Γ' are nearly constant for $r < r_*$, while Γ' is roughly constant for $r > r_*$. The prediction of Equation (34) using the values for the exponents at $r = 0$ is shown in the figure as the horizontal dotted line; it agrees well with the numerical results.

Figure (4) shows the exponent p in the size-linewidth relation, $v_T(r) \sim r^p$. The exponent is positive for $r > r_*$, but much smaller than the value $p = 1/2$ seen in simulations of non-self-gravitating turbulence. For $r < r_*$ the value of p quickly plunges to -0.5 , the value of a Keplerian profile. However, the normalization is below that of the Keplerian free-fall velocity as we discussed above. The predictions of the analytic theory, equations (A9) for $r < r_*$ and (A11) for $r > r_*$ are also shown, and agree well with the numerical results except in the immediate vicinity of r_* .

Figure (5) shows the result for p' ; the prediction $p' = -1/2$ for $r < r_*$ and the prediction of Equation (55) are shown as the dashed and dotted lines, respectively. Here we note again that the gravity from the central star drives the radial velocity to a Keplerian profile inside $r < r_*$; while we do not show it here, the magnitude of the infall velocity does not reach free-fall values.

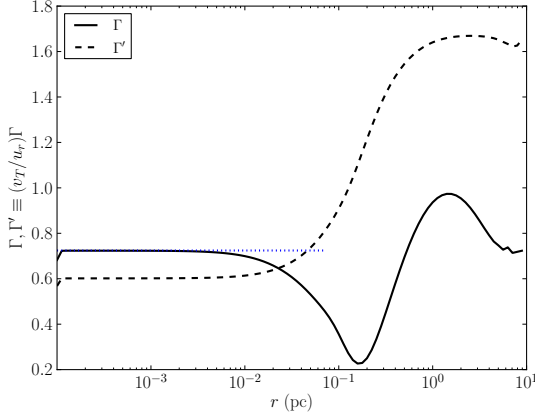


Figure 3. The run of $\Gamma(r)$ (solid line), and $\Gamma' \equiv (v_T/|u_r|)\Gamma(r)$ (dashed line). The prediction of equation (34) at $r = 0$, $\Gamma = \sqrt{8\eta^2/(5+4\eta^2)}$, for $r < r_*$ is shown as the horizontal dotted line.

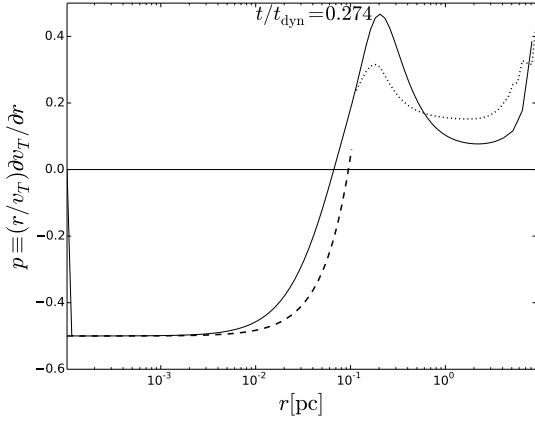


Figure 4. The run of $p(r)$, the exponent in the size-length relation (solid line), and the prediction of Equation (A9) for $r < r_*$ (dashed line), and of Equation (A11) for $r_* < r$ (dotted line).

Figure (6) plots the density exponent k_ρ (solid line) and the prediction of Equation (35) for $r < r_*$ (dashed line), and of Equation (53) for $r_* < r$ (dotted line). The prediction of $k_\rho = 1.5$ is recovered nicely in the numerical results.

Figure (7) shows the accreted mass versus $t - t_*$, with t_* defined to be the time when the accreted mass exceeds some minimum mass M_{\min} ; in the figure, $M_{\min} = 10^{-5}M_\odot$. Varying M_{\min} alters the appearance of the plot at early times but has no effect at later times. The mass increases in proportion to $(t - t_*)^2$, and the numerical result is in good agreement with the prediction of Equation (41).

We have calculated the run of density and velocity when the effects of a strong magnetic field, corresponding to a plasma $\beta = 1$ relative to ρv_T^2 , are included in the manner described above; in the notation of Equation (61), $\phi_B = 2$. The extra pressure provided by the magnetic field slows the infall, re-

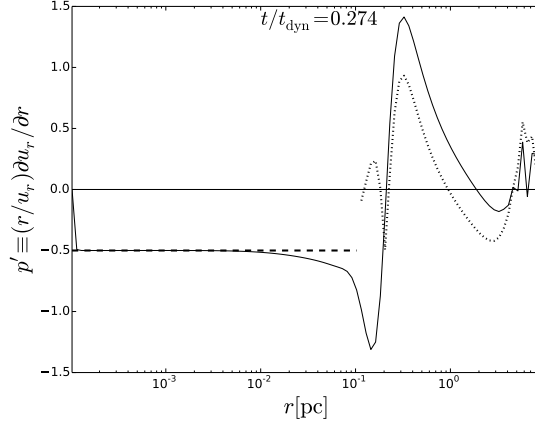


Figure 5. The run of $p'(r)$, where $u_r(r) = u_r(R)(r/R)^{p'}$ (solid line), and the prediction $p' = -1/2$ for $r < r_*$ (dashed line), and of Equation (55) for $r_* < r$ (dotted line).

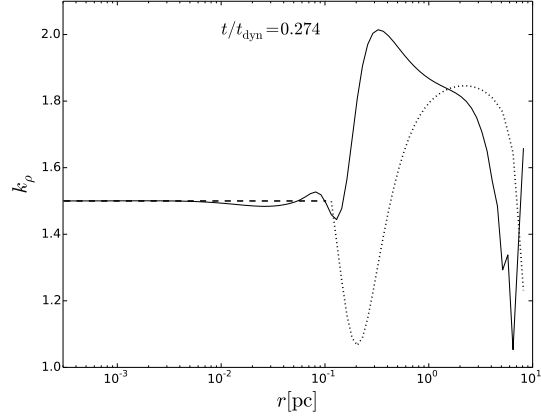


Figure 6. The run of $k_\rho(r)$, where $\rho(r) = \rho(R)(r/R)^{-k_\rho}$ (solid line), and the prediction of Equation (35) for $r < r_*$ (dashed line), and of Equation (53) for $r_* < r$ (dotted line).

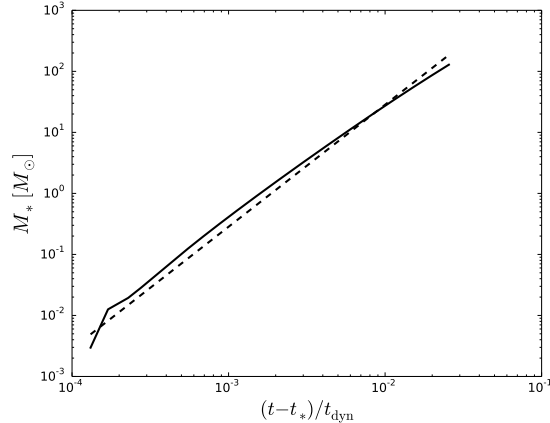


Figure 7. The accreted mass as a function of time since the star forms, $t - t_*$, where $t_*/\tau_{\text{dyn}} \approx 0.25$. The solid line is the numerical result, the dashed line is the prediction of Equation (41).

ducing the rate of accretion compared to a similar run with no magnetic pressure support by a factor of 1.9.

4. DISCUSSION

4.1. *The Connection Between Self-Gravity and the Size-Linewidth Relation*

Larson’s first law, the size-linewidth relation, applies to GMCs as well as to low mass star forming clumps. The power law index in GMC’s ($v_T(r) \sim r^p$) is almost universally observed to be $p \sim 0.4-0.5$, e.g., Larson (1981); Solomon et al. (1987); Heyer & Brunt (2004). The scaling relation extends to lower mass and smaller objects, e.g., Myers (1983), who finds $p \approx 0.5$.

In contrast, massive star forming regions show $p \approx 0.2$, and have much higher levels of turbulence at a given radius than is seen in low mass star formation regions, e.g., Fuller & Myers (1992); Caselli & Myers (1995); Plume et al. (1997). The turbulent velocities in these clumps are also much larger than the extrapolation of the GMC size-linewidth relation predicts. For example Plume et al. (1997) examine $r \sim 0.1 - 1$ pc clumps with masses $\sim 10^3 - 10^4 M_\odot$ selected on the basis of H₂O maser emission. They find turbulent velocities $v_T \approx 2 - 10$ km s⁻¹ (FWHM), nearly a factor of ten above Larson’s relation for $r \approx 0.3$ pc—see their Figure 5.

We have shown quantitatively how the conversion of gravitational potential energy into turbulent motion via adiabatic heating, coupled with the back pressure produced by that turbulence, can explain $p \approx 0.2$, for $r > r_*$, a result illustrated in Figure 4.

We can extract another prediction: in our model of converging flows, and in the simulations of Paper I, the density increases monotonically as r decreases. However, the turbulent velocity does not vary monotonically with r : at large radii ($r > r_*$) the turbulent velocity decreases as r decreases, but inside the critical radius, the turbulent velocity *increases* with decreasing r . It follows that a plot of turbulent velocity versus density for a single region will show that at low density the velocity decreases with increasing density, while at high density the velocity will increase with increasing density. In regions with different total mass, this breakpoint will occur at different radii. Even in regions with the same total mass, the break occurs at different radii, depending on the age of the system, since the critical radius depends on the mass of the central star or star cluster.

Plume et al. (1997) examine massive clusters and find that the linewidth increases with density. The gas densities they examine are very high, of order $n = 10^5$ to 10^7 cm⁻³. Their highest luminosity systems exceed $10^6 L_\odot$, which require stellar masses of order $3 \times 10^3 M_\odot$. They give a virial estimate of the total mass, finding values of order $5000 M_\odot$. This suggests that they may be resolving r_* in their most luminous objects.

Collapse models such as that of McLaughlin & Pudritz (1997); McKee & Tan (2003); Fatuzzo et al. (2004) predict $u_r(r)$, but they do not predict the run of $v_T(r)$ at any radius—they take it as an input. They assume that $v_T(r) \sim r^p$, with $p > 0$. Thus the linewidth will always decrease with increasing density, a corollary of the model that is inconsistent with the observations of Plume et al. (1997), a point those authors noted.

We interpret the finding that $p \approx 0.5$ in GMCs and low mass star formation regions to mean that GMCs, as a whole, are not undergoing rapid gravitational collapse. This is not to say that the virial parameter α_{vir} is larger than one; in the most massive GMCs, $\alpha_{\text{vir}} \sim 1$. Conversely, we interpret the observation that $p \approx 0.2 - 0.3$ in compact massive clumps to mean that they are the centers of large scale converging flows and are undergoing rapid gravitational collapse. We note that in the turbulent collapse model describe here the infall velocity should be substantially below the free-fall velocity, a point we return to below.

Papers reporting on simulations of turbulently stirred gas, in which the turbulence is maintained at a level corresponding to $\alpha_{\text{vir}} \approx 1$, often report the slope of the velocity power spectrum $P(\mathbf{k}) \equiv |v(\mathbf{k})|^2 \sim k^{-n_{3D}}$. This slope is related to the index p by the relation $p = (n_{3D} - 3)/2$, or if the one-dimensional power spectrum is used, $n_{1D} = n_{3D} - 2$, $p = (n_{1D} - 1)/2$. The implied values of $p = 0.45$ to 0.5 in hydrodynamic turbulence and $p = 0.45 - 0.6$ in MHD simulations (Padoan et al. 2007; Kritsuk et al. 2006; Collins et al. 2012); these simulations do not include gravity. However, even simulations which do include gravity find large values of n_{1D} , e.g., Collins et al. (2012), and by implication, large values of p .

Paper I (which included the effects of gravity) looked in the vicinity of local density maxima, which are undergoing collapse, and showed by direct measurement that $p \approx 0.2 - 0.3$, substantially smaller than the global average value in the same turbulent box. That paper also showed that the velocity power spectrum calculated in the immediate vicinity of a collapsing region has more power on small scales than the power spectrum calculated in exactly the same manner around random points in the same simulation box. The power spectrum, when calculated over an entire simulation box, is too crude a tool to detect the presence of collapsing flows.

4.2. *Slow, Radially Extended Infall*

The large turbulent pressure support which results from adiabatic heating tends to reduce the magnitude of the infall velocity, so that $|u_r(r)| \approx v_T(r) \approx -\Gamma \sqrt{GM_*/r}$ at small radii, and $|u_r(r)| \lesssim v_T(r) \approx \sqrt{GM(r)/r} \sim r^{+0.2}$ at large radii. The 3D simulations in Paper I show find a similar result (see Figure 9 in that paper). The slow increase of the turbulent velocity with increasing r (for $r > r_*$) is consistent with a modified Larson’s

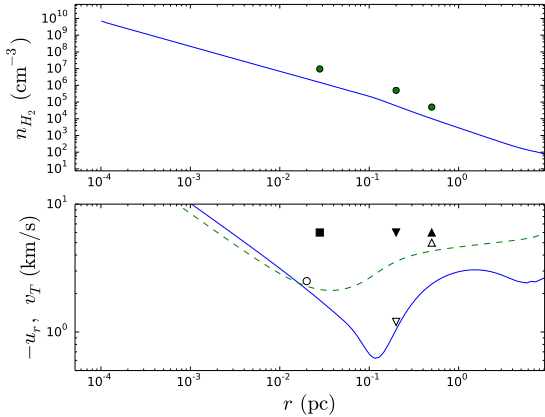


Figure 8. The density, infall, and turbulent velocity as a function of radius. The lines give the run of density (top panel), and of turbulent and infall velocity (dashed and solid lines respectively, in the bottom panel) in the run depicted in Figure 1, but at the time when the central mass $M_* = 89M_\odot$. The points in the upper panel are estimates of the density in the galactic massive star forming region G10.62-0.38. In order of increasing radius, the data is from Beltrán et al. (2011), Klaassen & Wilson (2008), and Ho & Haschick (1986). The points in the lower panel are measurements of v_T (filled symbols) and $-u_r$ (open symbols). In order of increasing radius, the measured value of $-u_r$ is represented by an open circle (Klaassen et al. 2011), a downward pointing open triangle (Klaassen & Wilson 2008), and an upward pointing open triangle (Ho & Haschick 1986). The filled square, downward filled triangle, and upward filled triangle are from Beltrán et al. (2011), Klaassen & Wilson (2008), and Ho & Haschick (1986); the observational papers do not provide an estimate of the errors in the turbulent velocity. The apparent dip in $-u_r$ around $r = 0.2$ pc is qualitatively consistent with the adiabatically heated turbulent collapse model.

first law, $p \approx 0.2$.

These findings contrast with the expanding collapse wave and related models, which predict that v_T , and hence the pressure, becomes negligible at small radii, and that the infall velocity reaches the free-fall value $u_r = -\sqrt{2GM_*/r}$. In fact this class of models predicts that $|u_r|$ decreases with increasing r at all radii, or, for expanding collapse wave models, falls to zero at a finite radius and remains there. The turbulent velocity is assumed to be an increasing function of r at all radii.

The different predictions of the infall models should allow us to distinguish between them. For example, Klaassen & Wilson (2008) see clear evidence of infall in line profiles of HCO^+ at $r = 0.3$ pc in G10.6-0.4, with $u_r = -1.0 \pm 0.1 \text{ km s}^{-1}$; see Figure 8. The infall extends inward to 0.03 pc as shown by Klaassen et al. (2011), who see inverse P Cygni profiles in CO lines and infer $u_r = -2.5 \text{ km s}^{-1}$. Ho & Haschick (1986) provide evidence for infall in the form of absorption in NH_3 at $r \approx 0.5$ pc, finding $v_T \approx 6 \text{ km s}^{-1}$ and $-u_r \approx 5 \text{ km s}^{-1}$.

Beltrán et al. (2011) estimate $v_T = 6 \text{ km s}^{-1}$ at $r = 0.04(D/6 \text{ kpc}) \text{ pc}$, and a rotational velocity $v_c = 2.1 \text{ km s}^{-1}$. Hence in this core, the turbulent pressure dominates both the rotational energy and

the kinetic energy of the infall, by a factor of 9 or more. Using the masses estimated below, it follows that the infall velocity is well below the free-fall velocity, by a factor of about two or three. This is evidence that something is slowing the infall. The fact that the turbulent velocity is substantially larger than the infall velocity suggests that turbulent pressure is responsible.

The bolometric luminosity of G10.6-0.4 is $L \approx 10^6 L_\odot$, and the stellar mass is therefore at least $M_* \approx 200M_\odot$ (Liu et al. 2011); if the stellar mass function in the proto-cluster is like the global initial mass function, the stellar mass could be a thousand solar masses. The gas mass on the scale of $1.5'' \approx 0.04 \text{ pc}$ is $M_g \sim 150M_\odot$ (Klaassen et al. 2009). The rough equality of stellar and gas masses suggests that the observations are probing sizes around r_* . This may explain the increase in the velocity inferred from -1 km s^{-1} at $r \approx 0.3 \text{ pc}$ to -2.5 km s^{-1} at 0.03 pc, while at the same time $|u_r| < \sqrt{2GM/r}$. The lines in Figure 8 come from the same model show in Figure 1, but at a later time, specifically, when $M_* \approx 90M_\odot$.

It is worth remarking that the innermost two data points in Figure 8 illustrate a similar phenomenon to that found in Plume et al. (1997); the density increases inward, while the turbulent velocity is flat or possibly slightly increasing inward.

We note that this observation of infall over a decade in radius, from $r \approx 0.03 \text{ pc}$ to 0.3 pc , and possibly to 0.5 pc , is consistent with the solutions found in this paper. This observation does not appear to be consistent with the predictions of the turbulent core model of McKee & Tan (2003), where the fiducial hydrostatic core radius $R_{\text{core}} = 0.05 \text{ pc}$, and the collapse proceeds from the inside out, i.e., the infall should be seen only for $r \lesssim R_{\text{core}}$.

In addition, the apparent increase of $|u_r|$ as r increases beyond 0.3 pc suggested by the observations of Ho & Haschick (1986) is inconsistent with collapse models.

4.3. The Star Formation Efficiency Per Free Fall Time

We have shown that the star formation rate in self-gravitating turbulent flows increases linearly in time in the absence of any feedback physics. This rapid growth in the star formation rate cannot continue for a dynamical time in real GMCs, since the fraction of gas converted into stars is seen to be less than 10–20% in the most extreme cases, and lower in many GMCs.

We suggest that the low observed star formation efficiency is due to two types of effects. The first is the effect of early (pre-supernovae) feedback from the newly formed stars, e.g., Murray et al. (2010).

The second is the effect of initial conditions; GMCs with large virial parameters will not form stars efficiently, since they will disperse in less than a GMC free-fall time. This dispersal cuts off the flow of gas to any collapsing regions in the cloud,

starving the nascent stars. Evidence for this is presented in paper I, in particular in Figure 14.

Recent papers on the star formation rate in 3D simulations have generally presented the result in terms of a constant value of ϵ_{ff} (e.g. Padoan & Nordlund 2011; Bate 2012; Krumholz et al. 2012b). The constant ϵ_{ff} that is reported in these papers is found by fitting a straight line to $M_*(t)$ at late times, typically a substantial fraction of a free-fall time after the first stars have formed. However, it is clear from examining the figures in these papers that $M_*(t)$ is increasing more rapidly than $\sim t$. Workers that have examined the early time behavior of the star formation rate in their simulations such as Myers et al. (2014) have found that ϵ_{ff} is not constant with time.

4.4. Long-lived Density Structures

The theory of adiabatically heated turbulent collapse predicts the existence of long-lived (compared to the local free-fall time) density structures. These structures are static in the sense that their shape does not change; however, they are dynamic in that fluid flows through them from large (multi-parsec) to small (milli-parsec) scales. For a significant fraction, of order one quarter, of the large scale dynamical time, these structures contain no newly formed stars. Seen in projection, or via extinction, they will have power-law surface density probability distribution functions. In the early phase, before the time we have denoted by t_* , the gas mass contained in the structure above a given column will increase with time; after t_* it will be constant.

Direct observational measurements of k_ρ are difficult, and exhibit a large range $1.0 \lesssim k_\rho \lesssim 2.0$, e.g., (van der Tak et al. 2000; Palau et al. 2014), making it difficult to distinguish between different theoretical models.

Regions in which $\rho(r) \sim r^{-k_\rho}$ will naturally produce extinction maps with powerlaw tails to the probability distribution of extinction (Kritsuk et al. 2011). There are only a handful of observational measurements of the surface density PDF, which should scale as $\Sigma \sim r^{-2/(k_\rho-1)}$. Power law tails have been seen in nearby star forming regions, e.g., Cambr esy (1999); Lada et al. (2009); Kainulainen et al. (2009). Lombardi et al. (2010) attribute this the effects of gravity. Kritsuk et al. (2011) perform numerical simulations of self-gravitating turbulence and find power-law tails in both the volume density and surface density distributions. They attribute these tails to collapsing regions. They also note that if the power law tail of the density PDF $\sim \rho^{-m}$ is produced by a run of density around density maxima $\rho(r) \sim r^{-k_\rho}$, then $m = 3/k_\rho$.

We agree with this interpretation, with the refinement that the outer layers of the star forming regions, before self-gravity becomes dominant, will have a run of density with $k_\rho = 1.6 - 1.8$, while the gravity-dominated inner region has $k_\rho = 1.5$. It is the turbulent pressure, not the self-gravity, that

produces $k_\rho > 1.5$, and hence density PDF tails that have $m < 2$.

4.5. Driving by Protostellar Jets

Low mass star forming regions show $p = 0.5$, similar to that in the ISM as a whole. Many such regions show prominent proto-stellar jets (Reipurth & Bally 2001), which are often suggested to be drivers of turbulence, e.g., Quillen et al. (2005). In his analytic models of turbulence driven by proto-stellar jets, Matzner (2007) finds $\sigma(r) \sim r^{1/2}$, i.e., $p = 0.5$ for $r < l$, where $l \approx 0.38$ pc is the characteristic size of a region subject to protostellar jets with fiducial properties. Simulations of jet driven turbulence (Carroll et al. 2009) find *steeper* spectra, $p \approx 0.87$. The theory does not predict $p \approx 0.2$ over an extended range of radii, whereas the observations show $p \lesssim 0.2$ for 0.04 pc $\lesssim r \lesssim 1.6$ pc, e.g., (Caselli & Myers 1995) or (Plume et al. 1997).

Heyer & Brunt (2004) note that $p \approx 0.5$ over a large range of scales and for low mass star forming regions, and argue that either jets produce a feature in $\sigma(r)$ around $r = l$, or the driving due to outflows is not important even at small scales. In fact, many low mass star forming regions, e.g., those studied by Myers (1983), fall on the original Larson relation, i.e. with the appropriate magnitude, indicating that neither jets nor conversion of infall energy to turbulence enhance the turbulence substantially over that expected from a simple extension of the behavior on larger scales.

The flat run of turbulent velocity seen in massive star forming regions, with no indication of a peak on scales of order a parsec, combined with the considerations above, suggest that the enhanced turbulence is not due to driving by proto-stellar jets.

4.6. Local Versus Global Collapse

The notion that there are coherent collapsing sub-structures in turbulent flows in which gravity is important has been suggested in the recent literature, e.g., Ballesteros-Paredes et al. (2011), and in particular Collins et al. (2012). The latter authors stress the existence of self-similar collapsing spheres at high density. Like Kritsuk et al. (2011), they measured density PDFs $P(\rho) \sim \rho^m$ with $m \approx 1.6 - 1.8$, and inferred $k_\rho = 3/m \approx 1.67 - 1.88$. It is these spheres, and their dynamics, that we model in this paper.

Ballesteros-Paredes et al. (2011) argue that “...the observational data are consistent with molecular clouds in a state of hierarchical and chaotic gravitational collapse, i.e. developing local centres of collapse throughout the whole cloud while the cloud itself is collapsing, and making equilibrium unnecessary at all stages prior to the formation of actual stars.”

We agree that local centers of collapse occur throughout the cloud. There is direct evidence for local collapse, on parsec scales, in the form of inverse P Cygni profiles seen toward known star forming

clumps (Di Francesco et al. 2001; Klaassen & Wilson 2008; Klaassen et al. 2011; Beltrán et al. 2011; van der Tak et al. 2013).

However, we disagree that GMCs (by which we mean clouds with $M \gtrsim 3 \times 10^5 M_\odot$ are collapsing globally. We are not aware of any detections of inverse P Cygni profiles toward GMCs on scales larger than $\lesssim 10$ pc, while the $10^6 M_\odot$ GMCs where the largest star clusters in the Milky Way form have radii of tens to a hundred parsecs. We would also point out that the Larson’s Law index p measured on large scales is $\sim 0.4 - 0.5$ (Larson 1981; Roman-Duval et al. 2011), substantially larger than that measured on small scales, typically $p \approx 0.1 - 0.2$ (Caselli & Myers 1995; Plume et al. 1997). If small values of p are taken as evidence for collapse around star forming regions, the large values of p seen on large scales must be taken as evidence against large scale collapse in GMCs. Given enough time, and in the absence of star formation, GMCs might collapse globally, but in the Milky Way this does not appear to be happening.

Vázquez-Semadeni et al. (2007) ran simulations in which two streams of gas were directed at each other; the subsequent collision generates turbulence. This is followed, after a dynamical time or two, by a global gravitational collapse. This collapse drives yet higher turbulent velocity, with the result that the global kinetic energy is thereafter similar in magnitude to the global gravitational energy. This is analogous to our result, but we are examining a local collapse, whereas theirs is a global result in a simulation containing a fairly large number of locally collapsing regions embedded in a globally collapsing cloud.

Vázquez-Semadeni et al. (2008) noted that in their simulations, regions around density maxima showed convergent flows, a result recovered in the simulations in paper I. They note in their section 6.1 that their diagnostic tools were not sufficient to decide whether the inflow was the cause or the consequence of gravitational contraction. We have shown that it is both—initially convergence leads to an over-density, and eventually to star formation, whose gravity then speeds the infall (increases the convergence) on small scales (inside r_*).

5. CONCLUSIONS

We have shown that turbulent self-gravitating flows with virial parameters near unity have the following properties:

The run of density asymptotes to

$$\rho(r, t) = \begin{cases} \rho(r_0) \left(\frac{r}{r_0}\right)^{-3/2}, & r < r_* \\ \rho(R, t) \left(\frac{r}{R}\right)^{-k_\rho}, & k_\rho \approx 1.6 - 1.8 \quad r > r_*. \end{cases} \quad (68)$$

Since k_ρ is fairly close to 1.5 at all radii, taking $r_0 = R$ is a fair approximation. The prediction that $\rho(r, t) \rightarrow \rho(r)$ for $r < r_*$ is in agreement with the

MHD and HD simulations in Paper I.

This run of density leads to a density PDF of the form $P(\rho) \sim \rho^{1.6-1.8}$ at high densities, and the related power law for the surface density PDF. This is in accord both with high resolution three dimensional MHD and hydro simulations (e.g. Kritsuk et al. 2011; Collins et al. 2012; Paper I), and with observational maps of visual extinction (e.g. Lada et al. 2009; Kainulainen et al. 2009).

The infall velocity

$$u_r(r, t) = \begin{cases} -\Gamma \sqrt{\frac{GM_*(t)}{r}}, \sim r^{-1/2} & r < r_* \\ -\Gamma \sqrt{\frac{GM(r, t)}{r}} \sim r^{0.2} & r > r_*, \end{cases} \quad (69)$$

where $\Gamma \approx 0.7$ at small radii, and $\Gamma \approx 1.0$ at large radii.

In contrast to most earlier models, the star forming clump is never in hydrostatic equilibrium. A clear test to decide between the two types of model is to measure the infall velocity over a large range of radii; both the expanding collapse wave model and the turbulent core model predict zero infall velocity at moderate radii (outside the collapse wave). We noted in §4.2 that there are some hints that the infall extends to $r \sim 0.5$ pc. Models that select solutions with finite infall velocities at large distance, e.g., Fatuzzo et al. (2004) predict lower values for the infall velocity at large radii, for a given mass accretion rate and run of density than the model presented here. In particular, they predict that $|u_r|$ decreases monotonically as r increases, whereas the adiabatically heated models predict that $|u_r|$ increases as r increases, for $r > r_*$.

The turbulent velocity

$$v_T(r, t) = \begin{cases} \frac{1}{2\eta} \Gamma \sqrt{\frac{GM_*(t)}{r}}, \sim r^{-1/2} & r < r_* \\ \frac{1.2}{\eta} \Gamma \sqrt{\frac{GM(r, t)}{r}} \sim r^{0.2} & r > r_*, \end{cases} \quad (70)$$

The result $p < 0$ for $r < r_*$ explains the observation of Plume et al. (1997) that the linewidth (v_T) increases with increasing density, a result that they noted was puzzling in the context of collapse models, since the latter assumed $p > 0$ at all radii.

The result that $p \approx 0.2$ for $r > r_*$ is the first explanation, to our knowledge, for the deviation from Larson’s law in massive clumps. In fact, both the larger magnitude of v_T at a given small distance, and the different slope p are in good agreement with observations. Both are the direct result of the conversion of infall kinetic energy and gravitational potential energy to turbulent motions as the accreting gas falls inward.

The stellar mass increases quadratically with time

$$M_*(t) = \phi M_{\text{cl}} \left(\frac{t - t_*}{\tau_{\text{ff}}}\right)^2. \quad (71)$$

The mass accretion rate

$$\dot{M}(r, t) = \begin{cases} 4\pi R^2 \rho(R) u_r(r, t), \sim t r^0 & r < r_* \\ 4\pi R^2 \rho(R) u_r(r, t) \sim t^0 r^{0.2} & r > r_* \end{cases} \quad (72)$$

It may be possible, with ALMA, to measure both the density (using different tracers) and the infall velocity over a range of radii in massive star forming clumps.

We would like to thank P. Klaassen for helpful conversations, and for sharing unpublished results. NM is supported by the Canada Research Chair program and by NSERC of Canada. PC acknowledges support from the NASA ATP program through NASA grant NNX13AH43G, and

NSF grant AST-1255469. This work was supported in part by the National Science Foundation under Grant No. PHYS-1066293 and the hospitality of the Aspen Center for Physics. Some of the computations were performed on the gpc supercomputer at the SciNet HPC Consortium (Loken et al. 2010). SciNet is funded by: the Canada Foundation for Innovation under the auspices of Compute Canada; the Government of Ontario; Ontario Research Fund - Research Excellence; and the University of Toronto. The authors acknowledge the Texas Advanced Computing Center (TACC) at The University of Texas at Austin for providing HPC resources that have contributed to the research results reported within this paper. URL: <http://www.tacc.utexas.edu>

APPENDIX

ESTIMATING THE INDEX p IN LARSON'S LAW

We estimate the power law index p in Larson's Law, for finite values of r , first for $r < r_*$ and then for $r > r_*$.

Estimating p Inside the Sphere of Influence ($r < r_$)*

We have shown in §2.3 that $\lim_{r \rightarrow 0} p = -1/2$. Here we extend the derivation to finite values, but still for $r < r_*$.

We start from the momentum Equation (13). Using Equation (47) and retaining the time derivative,

$$\frac{\tau_{\text{dyn}}}{\tau_{u_r}} + p' + \left(\frac{v_T}{u_r}\right)^2 (2p - k_\rho) + \frac{GM_*(t)/r}{u_r^2} = 0. \quad (A1)$$

The last term must vary slowly with r , so we find $p' = -1/2$, even at finite r . Since the continuity equation enforces $\partial\rho/\partial t = 0$, Equation (26) then ensures that $k_\rho = 3/2$ at finite r . However, the time derivative of the infall velocity is not zero, so $p(r)$ will depend on r .

Solving for $p(r)$,

$$p(r) = \frac{1}{2}k_\rho - \frac{1}{2}\left(\frac{u_r}{v_T}\right)^2 \left[\frac{\tau_{\text{dyn}}}{\tau_{u_r}} + p' + \Gamma^{-2}(0)\right], \quad (A2)$$

where $\Gamma(0)$ is given by Equation (34). Some algebra yields

$$p(r) = p(0) - \frac{1}{2}\left(\frac{u_r}{v_T}\right)^2 \frac{\tau_{\text{dyn}}}{\tau_{u_r}}. \quad (A3)$$

To evaluate this, we need an expression for $\tau_{\text{dyn}}/\tau_{u_r}$ at small but finite r . We start from Equation (33), and estimate

$$\frac{\partial u_r}{\partial t} \approx \frac{1}{2}u_r \frac{1}{M_*(t)} \frac{dM_*(t)}{dt}. \quad (A4)$$

Recall that

$$\frac{dM_*(t)}{dt} = -\lim_{r \rightarrow 0} 4\pi r^2 \rho(r, t) u_r(r, t), \quad (A5)$$

while from Equation (15) we have

$$4\pi r^2 \rho(r, t) = \frac{3 - k_\rho}{r} M_g(r, t). \quad (A6)$$

Using eqns. (A5) and (A6) in Equation (A4),

$$\frac{\partial u_r}{\partial t} \approx -\left(\frac{3 - k_\rho}{2}\right) \frac{u_r^2}{r} \frac{M_g(r, t)}{M_*(t)}. \quad (A7)$$

Thus

$$\frac{\tau_{\text{dyn}}}{\tau_{u_r}} \approx -\left(\frac{3 - k_\rho}{2}\right) \frac{M_g(r, t)}{M_*(t)} \approx -\frac{3}{4} \left(\frac{r}{r_*(t)}\right)^{3/2} \quad (A8)$$

for $r < r_*$.

Using this in Equation (A3),

$$p(r) \approx -\frac{1}{2} + \frac{3}{2}\eta^2 \left(\frac{r}{r_*}\right)^{3/2} \quad (\text{A9})$$

This prediction is shown in Figure (4) as the dashed line.

Estimating p Outside the Sphere of Influence ($r > r_$)*

The calculation of p for $r < r_*$ was greatly simplified by the fact that $\partial\rho/\partial t = 0$ inside the sphere of influence of the stars. Outside the sphere of influence, however, we cannot neglect the time variation of ρ , so the continuity equation becomes

$$\frac{\tau_{\text{dyn}}}{\tau_\rho} + 2 + p' - k_\rho = 0, \quad (\text{A10})$$

Combining eqns. (A10), (52), and (53), we find

$$p = \left[\frac{1}{2} - \frac{1}{(2\Gamma')^2} - \frac{1}{4} \left(\frac{u_r}{v_T}\right)^2 \left(\left| \frac{\tau_{\text{dyn}}}{\tau_\rho} \right| + \frac{\tau_{\text{dyn}}}{\tau_{v_T}} \right) \right] \left(1 - \frac{1}{2} \frac{u_r^2}{v_T^2} \right)^{-1}. \quad (\text{A11})$$

To use Equation (A11) to evaluate p , we need to estimate the time scale ratios, which depend on the outer boundary conditions. A simple estimate for the time scale over which the infall velocity changes is

$$\frac{\tau_{\text{dyn}}}{\tau_{u_r}} \approx 1. \quad (\text{A12})$$

The estimate for the density time scale has to take account of the outer boundary condition, since in our favored scenario, stars form in converging flows. At large scales in such flows $\rho(R) \approx \bar{\rho}$, where $\bar{\rho}$ is independent of time. Thus

$$\lim_{r \rightarrow R} \frac{\tau_{\text{dyn}}}{\tau_\rho} = 0. \quad (\text{A13})$$

At smaller radii, but still at radii large compared to r_* , we expect $|\tau_{\text{dyn}}/\rho| \leq 1$. Since the solution is scale invariant, we estimate

$$\left| \frac{\tau_{\text{dyn}}}{\tau_\rho} \right| \approx \left| \frac{\ln r/r_*}{\ln R/r_*} - 1 \right|. \quad (\text{A14})$$

From Equation (29), and anticipating that $p \ll 1$, we have

$$\left(\frac{v_T}{u_r}\right)^2 \approx \eta^2. \quad (\text{A15})$$

For our fiducial $\eta = 2/3$ and $\Gamma' = 1.6$, the denominator in Equation (A11) is roughly $3/4$; as a crude estimate we take $|\tau_{\text{dyn}}/\tau_\rho| = 1$, so

$$p \approx 4/3 \left[\frac{1}{2} - \frac{1}{10} - \frac{1}{4} \cdot \frac{1}{2} \cdot 2 \right] \approx 0.2 \quad (\text{A16})$$

as a very rough estimate.

REFERENCES

- Agertz, O., & Kravtsov, A. V. 2014, ArXiv e-prints, arXiv:1404.2613
 Ballesteros-Paredes, J., Hartmann, L. W., Vázquez-Semadeni, E., Heitsch, F., & Zamora-Avilés, M. A. 2011, MNRAS, 411, 65
 Bate, M. R. 2012, MNRAS, 419, 3115
 Beltrán, M. T., Cesaroni, R., Neri, R., & Codella, C. 2011, A&A, 525, A151
 Burbidge, E. M., Burbidge, G. R., Fowler, W. A., & Hoyle, F. 1957, Reviews of Modern Physics, 29, 547
 Cambrésy, L. 1999, A&A, 345, 965
 Carroll, J. J., Frank, A., Blackman, E. G., Cunningham, A. J., & Quillen, A. C. 2009, ApJ, 695, 1376
 Caselli, P., & Myers, P. C. 1995, ApJ, 446, 665
 Ceverino, D., Klypin, A., Klimek, E. S., et al. 2014, MNRAS, 442, 1545
 Collins, D. C., Kritsuk, A. G., Padoan, P., et al. 2012, ApJ, 750, 13
 Di Francesco, J., Myers, P. C., Wilner, D. J., Ohashi, N., & Mardones, D. 2001, ApJ, 562, 770
 Falgarone, E., Puget, J.-L., & Perault, M. 1992, A&A, 257, 715
 Fatuzzo, M., Adams, F. C., & Myers, P. C. 2004, ApJ, 615, 813
 Fuller, G. A., & Myers, P. C. 1992, ApJ, 384, 523
 Heiderman, A., Evans, II, N. J., Allen, L. E., Huard, T., & Heyer, M. 2010, ApJ, 723, 1019
 Heyer, M. H., & Brunt, C. M. 2004, ApJ, 615, L45
 Ho, P. T. P., & Haschick, A. D. 1986, ApJ, 304, 501

- Hopkins, P. F., Keres, D., Onorbe, J., et al. 2013, ArXiv e-prints, arXiv:1311.2073
- Kainulainen, J., Beuther, H., Henning, T., & Plume, R. 2009, *A&A*, 508, L35
- Kennicutt, Jr., R. C. 1998, *ApJ*, 498, 541
- Klaassen, P. D., & Wilson, C. D. 2008, *ApJ*, 684, 1273
- Klaassen, P. D., Wilson, C. D., Keto, E. R., & Zhang, Q. 2009, *ApJ*, 703, 1308
- Klaassen, P. D., Wilson, C. D., Keto, E. R., et al. 2011, *A&A*, 530, A53
- Knödseder, J. 2000, *A&A*, 360, 539
- Kritsuk, A. G., Norman, M. L., & Padoan, P. 2006, *ApJ*, 638, L25
- Kritsuk, A. G., Norman, M. L., & Wagner, R. 2011, *ApJ*, 727, L20
- Krumholz, M. R., Dekel, A., & McKee, C. F. 2012a, *ApJ*, 745, 69
- Krumholz, M. R., Klein, R. I., & McKee, C. F. 2012b, *ApJ*, 754, 71
- Lada, C. J., Lombardi, M., & Alves, J. F. 2009, *ApJ*, 703, 52
- . 2010, *ApJ*, 724, 687
- Larson, R. B. 1981, *MNRAS*, 194, 809
- Lee, E. J., Chang, P., & Murray, N. 2014, ArXiv e-prints, arXiv:1406.4148
- Leroy, A. K., Walter, F., Brinks, E., et al. 2008, *AJ*, 136, 2782
- Liu, H. B., Zhang, Q., & Ho, P. T. P. 2011, *ApJ*, 729, 100
- Loken, C., Gruner, D., Groer, L., et al. 2010, *Journal of Physics Conference Series*, 256, 012026
- Lombardi, M., Lada, C. J., & Alves, J. 2010, *A&A*, 512, A67
- Matzner, C. D. 2007, *ApJ*, 659, 1394
- McKee, C. F., & Tan, J. C. 2003, *ApJ*, 585, 850
- McLaughlin, D. E., & Pudritz, R. E. 1997, *ApJ*, 476, 750
- Murray, N. 2011, *ApJ*, 729, 133
- Murray, N., Quataert, E., & Thompson, T. A. 2010, *ApJ*, 709, 191
- Myers, A. T., Klein, R. I., Krumholz, M. R., & McKee, C. F. 2014, *MNRAS*, 439, 3420
- Myers, P. C. 1983, *ApJ*, 270, 105
- Myers, P. C., & Fuller, G. A. 1992, *ApJ*, 396, 631
- Myers, P. C., & Goodman, A. A. 1988, *ApJ*, 329, 392
- Padoan, P., & Nordlund, Å. 2011, *ApJ*, 730, 40
- Padoan, P., Nordlund, Å., Kritsuk, A. G., Norman, M. L., & Li, P. S. 2007, *ApJ*, 661, 972
- Palau, A., Estalella, R., Girart, J. M., et al. 2014, *ApJ*, 785, 42
- Plume, R., Jaffe, D. T., Evans, II, N. J., Martín-Pintado, J., & Gómez-González, J. 1997, *ApJ*, 476, 730
- Quillen, A. C., Thorndike, S. L., Cunningham, A., et al. 2005, *ApJ*, 632, 941
- Reipurth, B., & Bally, J. 2001, *ARA&A*, 39, 403
- Robertson, B., & Goldreich, P. 2012, *ApJ*, 750, L31
- Roman-Duval, J., Federrath, C., Brunt, C., et al. 2011, *ApJ*, 740, 120
- Shu, F. H. 1977, *ApJ*, 214, 488
- Solomon, P. M., Rivolo, A. R., Barrett, J., & Yahil, A. 1987, *ApJ*, 319, 730
- Trujillo-Gomez, S., Klypin, A., Colin, P., et al. 2013, ArXiv e-prints, arXiv:1311.2910
- van der Tak, F. F. S., van Dishoeck, E. F., Evans, II, N. J., & Blake, G. A. 2000, *ApJ*, 537, 283
- van der Tak, F. F. S., Chavarría, L., Herpin, F., et al. 2013, *A&A*, 554, A83
- Vázquez-Semadeni, E., Gómez, G. C., Jappsen, A. K., et al. 2007, *ApJ*, 657, 870
- Vázquez-Semadeni, E., González, R. F., Ballesteros-Paredes, J., Gazol, A., & Kim, J. 2008, *MNRAS*, 390, 769
- Wu, J., Evans, II, N. J., Gao, Y., et al. 2005, *ApJ*, 635, L173